Title	Development of U-Pb dating of uraninite using a secondary ion mass spectrometer: Selection of reference material and establishment of calibration method
Authors	Kenji Horie, Hiroshi Hidaka
Citation	Island Arc, 28(5), 1-16, 2019
Issue Date	2019-7-23
Type	Journal Article
URL	https://doi.org/10.1111/iar.12319
Right	
Textversion	publisher

Received: 14 December 2017 | Revised: 26 February 2019 | Accepted: 20 May 2019

DOI: 10.1111/iar.12319

RESEARCH ARTICLE

Island Arc WILEY

Development of U–Pb dating of uraninite using a secondary ion mass spectrometer: Selection of reference material and establishment of calibration method

Kenji Horie[1,2] | Hiroshi Hidaka[3]

[1]Geoscience Research Group, National Institute of Polar Research, Tachikawa, Japan

[2]Department of Polar Science, The Graduate University for Advanced Studies (SOKENDAI), Tachikawa, Japan

[3]Department of Earth and Planetary Scicences, Graduate School of Environmental Studies, Nagoya University, Nagoya, Japan

Correspondence
Kenji Horie, National Institute of Polar Research 10-3, Midori-cho, Tachikawa-shi, Tokyo 190-8518, Japan.
Email: horie.kenji@nipr.ac.jp

Funding information
Japan Society for the Promotion of Science, Grant/Award Numbers: Grant-in-Aid for JSPS Fellows No.05203, Grant-in-Aid for JSPS Fellows No.06290, Grant-in-Aid for Scientific Research No.17204051

Abstract

A method for U–Pb isotopic dating using secondary ion mass spectrometer (SIMS) was developed for uraninite. Correlation between $^{251}(UO)^+/^{235}U^+$ and $^{206}Pb^+/^{235}U^+$ obtained by a sensitive high-resolution ion microprobe (SHRIMP) was adopted for a calibration from secondary ion ratios (Pb^+/U^+) to the atomic abundance ratios (Pb/U). In this study, a uraninite sample ($^{206}Pb/^{238}U$ = 0.1647) collected from Faraday mine, Bancroft, Canada, is used as a reference material for the U–Pb calibration. The established method was applied to three uraninite samples collected from the Chardon, Ecarpière, and Mistamisk mines. The calibrated $^{206}Pb^*/^{238}U$ ratios of the three uraninites show correlation with Pb/U elemental ratios obtained using an electron probe microanalyzer (EPMA) (correlation coefficients: 0.98, 0.99, and 0.97, respectively), which indicates the reliability of the SHRIMP calibration method used in this study. The analysis of Ecarpière uraninite provides concordant U–Pb data, and a weighted average of the $^{206}Pb^*/^{238}U$ age is 287 Ma ±8 Ma (95 % conf.) which is consistent with the previous chronological results by SIMS. Mistamisk uraninite provides discordant U–Pb data with the upper and lower intercept ages of 1 729 and 421 Ma, which correspond to uraninite formation in association with the Hudsonian orogeny and the remobilization of uranium as pitchblende, respectively. The U–Pb age of Chardon uraninite (315 Ma) is consistent with the igneous activity of Mortagne granite, but is older than the previously reported age (264 Ma). Marcasite in the Chardon uraninite altered to goethite under the oxidizing condition, which indicates that U–Pb system in the uraninite crystallized at 315 Ma was disturbed under the oxidizing condition. The established calibration method using Faraday uraninite is useful for U–Pb isotopic dating on the scale of a few micrometers to tens of micrometers, which make it possible to obtain the accurate age of uraninite.

KEYWORDS
reference material, secondary ion mass spectrometry, U–Pb dating, uraninite

1 | INTRODUCTION

U–Pb dating of uraninite and pitchblende (UO_2 – U_3O_8) provides valuable information on the formation of uranium deposits (e.g., Förster & Haack, 1996; Kotzer & Kyser, 1993) and on the elemental mobilization association with the alteration in uraninite. The understanding of uranium mobilization provides important information on studies of the safe disposal of radioactive wastes from nuclear plants

(e.g., Hidaka, Horie, & Gauthier-Lafaye, 2007; Horie & Hidaka, 2004). Moreover, the timing of uranium mineralization from the Archean to the Paleoproterozoic period is a good indicator of atmospheric oxygen evolution because uranium is mobilized as a uranyl ion ($[UO_2]^{2+}$) only under oxidizing conditions (e.g., Bekker et al., 2004; Holland, 1984, 1999).

The chronological studies on uraninites have been carried out by chemical dating, Pb isotopic dating and U–Pb dating. In the first reports on absolute age determination in geology, the chronological studies on uraninite were carried out by applying chemical dating (e.g., Holmes, 1911). The chemical dating is still a useful technique with an electron probe microanalyzer (EPMA) for U and Th rich minerals, such as monazite in magmatic, metamorphic, and sedimentary rocks (e.g., Braun, Montel, & Nicollet, 1998; Cocherie & Albarede, 2001; Cocherie, Legendre, Peucat, & Kouamelan, 1998; Montel, Veschambre, & Nicollet, 1994; Rhede, Wendt, & Förster, 1996; Suzuki & Adachi, 1991; Suzuki, Adachi, & Kajizuka, 1994; Suzuki, Adachi, & Tanaka, 1991). The advantage of microanalysis is that it enables us to make measurements of ages on the scale of a few micrometers to tens of micrometers, considering mineralogical features. Chemical dating by using EPMA is useful for uraninite as the uraninite sometimes shows complex chemical texture resulted by multistage mineralization and alteration (e.g., Bowles, 1990; Förster, 1999; Kempe, 2003). However, only few studies on the chemical dating of uraninite have been carried out (e.g., Bowles, 1990; Förster, 1999; Kempe, 2003; Parslow, 1982; Yokoyama, Shigeoka, Otomo, Tokuno, & Tsutsumi, 2016). Significant problems arising in chemical dating by using EPMA analysis are as follows: (i) The common Pb correction cannot be applied; (ii) It is difficult to consider the redistribution of U and Pb compared with isotopic dating because EPMA analysis cannot determine the isotopic ratio, such as $^{207}Pb/^{206}Pb$, $^{206}Pb/^{238}U$, and $^{207}Pb/^{235}U$, which enable us to find discordant data. Thus, it is difficult to study the disturbance in a U–Pb system in uraninite. Usually, concordant U–Pb data of uraninite is not obtained by Pb loss, recrystallization, and the change in the chemical composition due to the alteration enhanced by radiation damage. In order to address these issues and to discuss the exact and detailed age of uraninite, U–Pb isotopic dating has to be carried out on the scale of a few micrometers to tens of micrometers using secondary ion mass spectrometers.

Over the past three decades, the isotopic analysis of uraninite by secondary ion mass spectrometry (SIMS) has provided precise chronological information on the migration of uranium in association with geological events (Cathelineau, Boiron, Holliger, & Poty, 1990; Evins, Sunde, Schöberg, & Fayek, 2001; Fayek, Harrison, Ewing, Grove, & Coath, 2002; Fayek, Harrison, Grove, & Coath, 2000; Fayek, Kyser, & Riciputi, 2002; Fourel, Lancelot, Allegre, & Dupre, 1988; Holliger, 1988, 1992, 1994; Holliger & Cathelineau, 1986, 1987, 1988; Horie & Hidaka, 2004; Horie, Hidaka, & Gauthier-Lafaye, 2004; Meddaugh, 1983). The calculation of the $^{206}Pb/^{238}U$ age by SIMS analysis is generally complicated by the fact that the ionization efficiency of secondary ions varies mainly with the chemistry and the structure of the target minerals. To correct this effect, a suitable calculation method and reference materials are required to calibrate the measured secondary ion ratio (Pb^+/U^+) to the atomic abundance ratio (Pb/U). In the U–Pb isotopic analysis of uraninite, the relative sensitivity factor (RSF) approach is employed to calculate Pb/U (Fayek, Kyser, & Riciputi, 2002; Holliger, 1988). Holliger (1988) has suggested a linear correlation between ($^{206}Pb/^{238}U$) and ($^{206}Pb^+/^{270}[UO_2]^+$) in pitchblendes and uraninites on the basis of experimental results. Fayek, Kyser, and Riciputi (2002) have introduced another calibration method that is based on the exponential correlation between ($^{206}Pb/^{238}U$) and ($^{206}Pb^+/^{238}U^+$). However, it has been reported that it is difficult to achieve highly accurate calibration of Pb/U using the RSF approach. For example, even if a target material has homogeneous Pb/U, Pb^+/U^+ differs in the analyzed regions, particularly if a high primary ion current is used (e.g., Williams, 1998).

The highly accurate calibration on zircon U–Pb dating has been established using a sensitive high-resolution ion microprobe (SHRIMP), providing precise magmatic ages and detailed thermal history of crustal materials (e.g., Compston, Williams, & Meyer, 1984; Stern, 1998; Williams, 1998). For the analysis with SHRIMP, the empirical relationship observed between $^{206}Pb^+/^{238}U^+$ and $^{254}(UO)^+/^{238}U^+$ has been conventionally used for the calibration of Pb/U. Compston et al. (1984) have proposed a linear correlation for the calibration and determined the Pb/U ages of the lunar highland breccias. This relationship has been considered to obey a power law of the form $^{206}Pb^+/^{238}U^+ = a(^{254}(UO)^+/^{238}U^+)^2$ (Claoué-Long, Compston, Roberts, & Fanning, 1995). Stern and Amelin (2003) have reported that the calibration using the relationship between $^{206}Pb^+/^{270}(UO_2)^+$ and $^{254}(UO)^+/^{238}U^+$ reduces the analytical uncertainties in the $^{206}Pb/^{238}U$ ratios. A similar calibration approach is applicable to several types of U-bearing minerals such as monazite (e.g., DeWolf, Belshaw, & O'Nions, 1993; Williams, Buick, & Cartwright, 1996), titanite (e.g., Horie, Hidaka, & Gauthier-Lafaye, 2008; Kinny, McNaughton, Fanning, & Maas, 1994), baddeleyite (e.g., Wingate, Campbell, Compston, & Gibson, 1998), and apatite (e.g., Horie et al., 2008; Sano, Oyama, Terada, & Hidaka, 1999).

The calibration from Pb^+/U^+ to Pb/U requires a matrix-matched reference material which has a homogeneous and concordant $^{206}Pb*/^{238}U$ ratio (Pb* indicates the radiogenic Pb portion) from the submicrometer to the intergranular scale. However, finding a uraninite sample used as the reference material for the U–Pb analysis appears to be difficult as the U–Pb system of uraninite is often disturbed by the rapid Pb diffusion in uraninite (Brandt & Pershinov, 1968; Janeczek & Ewing, 1995; Yershov, 1974) and the high solubility of uranium under oxidizing conditions (e.g., Langmuir, 1978). In addition, the redistribution of Pb in the uranium matrix may be considerably enhanced by the radiation damage due to the α-decay of U. In this study, we evaluate possible reference materials for SHRIMP uraninite U–Pb dating.

In order to eliminate ambiguities due to the calibration and matrix effects in SIMS analysis, Meddaugh (1983) has suggested another technique, which has been refined by Fayek et al. (2000), that combines the SIMS analysis of the Pb isotopic composition and the EPMA analysis of Pb/U elemental ratio, and provides the U–Pb

concentrations without the calibration of the secondary ion yields for U^+ and Pb^+. The Pb concentration can be analyzed using EPMA with a stable Pb reference material, such as natural crocoite ($PbCrO_4$) or even pure Pb metal. The disadvantages of this analytical method are that (i) exactly the same spots must be analyzed in both the EPMA and SIMS, which is difficult and also increases the efforts involved; (ii) the sampled volumes in the EPMA and SIMS analyses are usually different; and (iii) this method cannot be applied to samples that have undergone nuclear reactions, such as the Oklo uranium deposit at Gabon.

In this study, we try to establish a calibration method for the U–Pb isotopic analysis of uraninite using SHRIMP. We utilize the calibration method similar to that used in the SHRIMP zircon U–Pb dating. As compared to the RSF approach, more accurate results are obtained with an appropriate reference material and calibration method. In order to validate the calibration method, the U–Pb analyses are carried out for three uraninite samples from the Chardon, Ecarpière, and Mistamisk mines.

2 | SAMPLE DESCRIPTION

2.1 | Faraday uraninite

The uraninite sample collected from the Faraday mine, Madawaska, Maine, U.S.A. is used as the reference material for the calibration of U–Pb uraninite analysis by SHRIMP. Faraday uraninite is deposited along the boundary between a belt of metagabbro and amphibolite and the Faraday granite at Bancroft, Ontario, Canada. The metagabbro and amphibolite were emplaced into the supracrustal rocks of the Grenville Supergroup in the middle Proterozoic period. The ore bodies, mainly consisting of uraninite and uranothorite, are a part of a system of pegmatitic pyroxene granite dykes found at intervals of over 2000 m with a width of about 100 m (Leng, Griffith, & Steacy, 1962). The boundaries between the granite dykes and the host rocks are usually sharp, and the ores are usually confined within the dykes. The crystallization age of Faraday uraninite is 1 045 Ma ±30 Ma (Pb isotopic dating; Robinson, 1960). Faraday uraninite has a characteristically higher Th/U ratio (0.11) as compared to other uraninites found in Ontario and Quebec (Robinson & Sabina, 1955). The sample used in this study is a fragment of a massive uraninite grain.

2.2 | Chardon and Ecarpière uraninites

Chardon and Ecarpière uraninite deposits developed along the northern contact of Mortagne leucogranite in the southeast of the Armoricain Massif, France, where peraluminous magmatism occurred at approximately 340 to 300 Ma (Bernard-Griffiths, Peucat, Sheppard, & Vidal, 1985; Vidal, 1973, 1980). The intrusion age of Mortagne granite has been estimated to be 310 Ma ±10 Ma (Sonet, 1967) and 313 Ma ±5 Ma (Guineberteau, 1986) by the Rb–Sr method. Uranium mineralization in this region occurred in extensional hydraulic fractures (opening and brecciation by pressurized fluid), and is related to the tectonic deformation along the South Armorican Shear Zone that took place during the Hercynian orogeny (Cathelineau, 1981; Cathelineau et al., 1990; Cathelineau & Leroy, 1981; Lillié, 1974). Detailed paragenetic sequences in the Chardon and Ecarpière mines were reported in mineralogical studies (e.g., Cathelineau, 1981; Cathelineau & Leroy, 1981; Poty et al., 1986) and consist of (i) quartz; (ii) pitchblende + pyrite; (iii) quartz + hematite; and (iv) the axial filling of veins which mainly consists of silica and dolomite. Previous study suggests multistage U mineralization in the Chardon and Ecarpière mines (Cathelineau et al., 1990). Major mineralization in the Ecarpière mine has been determined to have occurred at 286 Ma ±7 Ma by using U–Pb dating of pitchblende by CAMECA IMS 3f microprobe (Cathelineau et al., 1990). The U–Pb analyses of Chardon uraninite by TIMS and SIMS have yielded the upper and lower intercept ages to be 264 ±9 and 110 Ma, respectively (Cathelineau et al., 1990). In previous studies, it has been concluded that the U mineralization in the Chardon and Ecarpière mines occurred 30 Ma– 60 Ma after the intrusion of Mortagne granite.

2.3 | Mistamisk uraninite-albite veins

The Mistamisk Valley is located in the central part of the Labrador Trough, which is a Proterozoic basin in Quebec, Canada. The Labrador Trough is bordered by the Archean gneisses of the Superior Province to the west, by the high-grade metamorphic rocks of the Grenville Province to the south, and by the Proterozoic and Archean gneisses belt to the east. The western part of the trough is mainly composed of clastic and chemical sediments deposited on the Archean gneisses, whereas the eastern part mainly consists of basaltic and gabbroic rocks. The Mistamisk Valley transects basalt and gabbro bodies, and is covered by the fine-grained clastic and chemical sediments (Dimroth, 1978). The volcanic rocks were thrust over the sedimentary rocks during the Hudsonian orogeny (Dimroth, 1978). The uraniferous veins in the Mistamisk Valley are located in the metasediments of the western part of the trough, and mainly consist of albite, uraninite, dolomite, and chlorite. Uraninite is generally concentrated in the axial part of the veins, and is fractured and recemented by albite and carbonate. The U–Pb data for the uraninite obtained by a conventional U–Pb isotopic method indicate that uraninite crystallized at ca. 1 800 Ma, which is consistent with the Hudsonian orogeny, and the remobilization of uranium as pitchblende occurred at ca. 400 Ma (Kish & Cuney, 1981). From the SIMS analysis of uraninite, Holliger (1988) has reported that the crystallization age of uraninite is 1 724 Ma ±7 Ma.

3 | ANALYTICAL PROCEDURES

3.1 | EPMA analysis

Faraday uraninite was mounted with the Chardon, Ecarpière, and Mistamisk uraninites using epoxy resin, and polished using 1 μm diamond paste. Mineralogical observation was carried out by using scanning electron microscope (SEM; JEOL JSM-5400) with energy dispersive spectrometer (EDS; Link QX2000) at the National Museum of Nature

and Science (NMNS), Japan, and by micro-Raman spectroscopy (Renishaw inVia Raman Reflex microscope) at Hiroshima University. The detailed analytical procedures of Raman spectroscopy can be found in Horie, Hidaka, and Gauthier-Lafaye (2006).

EPMA (JEOL JXA-8800) at NMNS were used for the quantitative analysis of major elements and for capturing the backscattered electron (BSE) images of the uraninite samples. Prior to the quantitative analysis, the qualitative analysis was carried out by using SEM-EDS to select elements to be analyzed. In this study, the quantitative analysis followed the techniques proposed by Montel, Foret, Veschambre, Nicollet, and Provost (1996), Santosh, Yokoyama, Biju-Sekhar, and Rogers (2003), and Suzuki and Adachi (1991, 1994). The analysis was carried out to determine U, Th, Pb, Si, Ca, and rare earth elements. The Si and Ca were included in the EPMA analysis as high concentrations of those elements were detected with SEM-EDS analysis of alteration phases in the uraninite (Kempe, 2003).

The typical analytical conditions of the EPMA analysis were a spot size of 5 μm and electron beam current of 500 nA at acceleration voltage of 15 kV. The counting times (peak + background) for Pb, U, Th, and all other elements were 130, 70, 80, and 20 s, respectively. The reference materials for U, Th, and Pb were synthesized UO_2, ThO_2, and natural crocoite ($PbCrO_4$), respectively. For the other elements, the reference materials were the end-member synthetic phosphates (XPO_4) for the rare earth elements and Y, wollastonite for Ca and Si, albite for Na, and fluorite for F. The X-ray lines used were U$M\alpha$, Th$M\alpha$, Pb$M\alpha$, Ce$L\alpha$, Nd$L\beta$, Sm$L\alpha$, Gd$L\beta$, Dy$L\alpha$, Er$L\alpha$, Yb$L\alpha$, Y$L\alpha$, Ca$K\alpha$, Si$K\alpha$, Na$K\alpha$, and F$K\alpha$. PRZ corrections (modified ZAF) were applied to the analyses. The spectral interference of Y$L\gamma$ on Pb$M\alpha$ and of Th$M\beta$ on U$M\alpha$ was corrected. Problems generally arise in accurate determination in the EPMA analyses for F and Na because of the several factors, such as anisotropic diffusion (e.g., Stormer, Pierson, & Tacker, 1993). However, this effect has not been observed by Peng, Luhr, and McGee (1997), and we assume that the diffusion does not significantly affect our results.

3.2 | Inductively coupled plasma–mass spectrometry (ICP–MS) analysis

Faraday uraninite was crushed and six fragments approximately 10 mg each were dissolved in 2 M HNO_3. Six solutions were obtained and were individually diluted to 15 mL with 0.5 M HNO_3, and the U and Pb contents in the solutions were then measured by ICP–MS (Micromass PQ III) at Hiroshima University in order to confirm the homogeneity of the Pb/U contents between the fragments. The details of analytical procedures are in Takahashi et al. (2002).

3.3 | SHRIMP analysis

Prior to SHRIMP analysis, analytical spots are selected by BSE observation and quantitative analysis using EPMA in order to find pure uraninite phases without any altered domains. The U–Pb isotopic analyses were performed using the SHRIMP-II instrument at Hiroshima University. An O_2^- primary ion beam of around 0.5 nA was used to sputter an analytical spot of about 5 μm in diameter on polished uraninite grains. The analytical condition for the U–Pb dating of uraninite using SHRIMP was similar to that of the U–Pb zircon analyses carried out by Compston et al. (1984), Stern (1998), and Williams (1998), though $^{235}U^+$ and $^{251}(^{235}U^{16}O)^+$ instead of ^{238}U and $^{254}(^{238}U^{16}O)^+$ were measured as the high U concentration in the samples. A mass resolution of 6 000 (M/ΔM at 1 % of peak height) was used to determine the $^{204}Pb^+$, $^{206}Pb^+$, $^{207}Pb^+$, $^{208}Pb^+$, $^{235}U^+$, $^{248}(ThO)^+$, and $^{251}(UO)^+$ peaks in the U–Pb analysis. Fayek, Kyser, and Riciputi (2002) pointed out the interference of the hydrides of ^{206}Pb and ^{207}Pb on ^{207}Pb and ^{208}Pb, respectively. The sample resin was maintained under high vacuum (< 3.0×10^{-8} Torr) in a sample chamber, and $^{209}(^{208}PbH)^+$ was monitored to assess the isobaric interference on the Pb isotopic composition.

In this study, the instrumental mass fractionation (IMF) of the Pb isotopes in the uraninite was not corrected as the IMF was negligibly small (Evins et al., 2001; Fayek, Kyser, & Riciputi, 2002; Holliger & Cathelineau, 1988; Meddaugh, 1983). The small IMF of Pb isotope was also estimated by that of U in uraninite (4.4 ‰/amu; Horie et al., 2004).

Analytical data were processed using the PRAWN-LEAD program of SHRIMP system. A correction for common Pb was made on the basis of the measured ^{204}Pb and the model for common Pb compositions proposed by Cumming and Richards (1975). The pooled ages presented in this paper were calculated by Isoplot/Ex (Ludwig, 2003).

4 | RESULTS AND DISCUSSION

4.1 | Faraday uraninite as reference material

4.1.1 | Chemical composition and homogeneity of samples

The BSE image of the entire fragment of Faraday uraninite shown in Figure 1 reveals that the sample appears homogeneous and does not

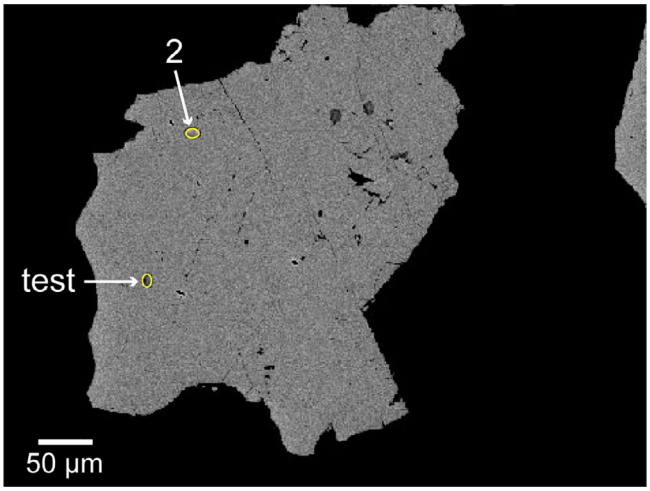

FIGURE 1 Backscattered electron (BSE) image of Faraday uraninite. White circles indicate SHRIMP spots. Dark pits and linear scratches are resulted by surface roughness

contain inclusions. Table 1 presents the chemical compositions of the major elements in Faraday uraninite. Low analytical totals ranging between 90.96 and 96.69 wt% may be caused by the presence of elements not included in the analysis such as H_2O. As shown in Figure 2, a correlation between the UO_2 contents and the analytical totals suggests that the difference is also caused by the presence of

TABLE 1 Chemical composition of major elements in Faraday uraninite

	1	2	3	4	5	6	7	8	9	10
UO_2	63.29	61.08	62.73	60.28	61.47	62.12	61.10	60.64	61.95	59.36
ThO_2	18.71	18.84	17.47	19.10	18.13	17.92	19.09	18.84	17.00	18.83
PbO	11.17	10.83	10.99	10.74	10.93	11.06	10.83	10.78	10.93	10.04
CaO	0.19	0.18	0.30	0.18	0.13	0.18	0.22	0.18	0.17	0.44
SiO_2	n.d.	n.d.	0.03	0.01	n.d.	n.d.	0.01	n.d.	0.02	0.18
Ce_2O_3	0.50	0.54	0.52	0.57	0.49	0.46	0.64	0.73	0.68	0.64
Nd_2O_3	0.43	0.51	0.45	0.47	0.50	0.46	0.53	0.50	0.47	0.47
Sm_2O_3	0.09	0.13	0.07	0.12	0.08	0.07	0.06	0.08	0.10	0.11
Yb_2O_3	0.10	0.13	0.08	0.12	0.09	0.11	0.08	0.09	0.08	0.06
Er_2O_3	0.14	0.18	0.12	0.20	0.22	0.16	0.20	0.19	0.18	0.14
Dy_2O_3	0.19	0.16	0.16	0.12	0.18	0.20	0.17	0.17	0.17	0.10
Gd_2O_3	0.08	0.06	0.07	0.12	0.10	0.09	0.10	0.08	0.10	0.06
Y_2O_3	0.51	0.67	0.45	0.54	0.64	0.48	0.64	0.50	0.59	0.54
Total	95.40	93.31	93.43	92.57	92.95	93.31	93.67	92.77	92.43	90.96
(Atomic wt%)										
U	55.79	53.84	55.30	53.14	54.18	54.76	53.86	53.45	54.61	52.32
Th	16.44	16.56	15.35	16.79	15.93	15.75	16.78	16.56	14.94	16.55
Pb	10.37	10.05	10.20	9.97	10.14	10.26	10.05	10.00	10.14	9.32
Pb/U	0.1858	0.1867	0.1845	0.1876	0.1872	0.1874	0.1866	0.1872	0.1858	0.1781
Th/U	0.2947	0.3075	0.2776	0.3159	0.2940	0.2876	0.3115	0.3098	0.2736	0.3163
	11	**12**	**13**	**14**	**15**	**16**	**17**	**18**	**19**	**20**
UO_2	61.17	64.73	63.73	61.06	61.53	62.91	60.89	64.16	62.33	63.58
ThO_2	18.53	17.67	17.28	18.93	17.86	17.71	19.80	17.81	18.15	17.01
PbO	10.84	11.48	11.30	10.79	10.86	11.14	10.85	11.34	11.08	11.20
CaO	0.14	0.20	0.20	0.09	0.18	0.09	0.13	0.15	0.22	0.18
SiO_2	0.02	n.d.	0.02	0.03	0.01	n.d.	n.d.	n.d.	0.01	0.01
Ce_2O_3	0.51	0.63	0.52	0.58	0.71	0.73	0.61	0.60	0.64	0.65
Nd_2O_3	0.46	0.52	0.45	0.52	0.70	0.71	0.59	0.55	0.61	0.63
Sm_2O_3	0.10	0.11	0.09	0.18	0.18	0.23	0.13	0.20	0.21	0.20
Yb_2O_3	0.09	0.09	0.07	0.09	0.11	0.13	0.11	0.10	0.10	0.10
Er_2O_3	0.16	0.17	0.15	0.19	0.22	0.24	0.24	0.19	0.25	0.22
Dy_2O_3	0.27	0.26	0.34	0.40	0.40	0.42	0.44	0.33	0.43	0.43
Gd_2O_3	0.22	0.30	0.39	0.41	0.40	0.40	0.45	0.32	0.42	0.41
Y_2O_3	0.54	0.54	0.57	0.62	0.66	0.62	0.54	0.62	0.56	0.56
Total	93.04	96.69	95.11	93.90	93.82	95.33	94.76	96.35	95.01	95.18
(Atomic wt%)										
U	53.92	57.06	56.18	53.82	54.24	55.46	53.67	56.56	54.94	56.05
Th	16.28	15.53	15.19	16.64	15.70	15.56	17.40	15.65	15.95	14.95
Pb	10.06	10.66	10.49	10.01	10.08	10.34	10.07	10.53	10.29	10.39
Pb/U	0.1866	0.1868	0.1867	0.1860	0.1858	0.1864	0.1877	0.1862	0.1873	0.1854
Th/U	0.3020	0.2721	0.2703	0.3091	0.2894	0.2806	0.3242	0.2767	0.2903	0.2667

n.d., not detected.
All data in wt%.

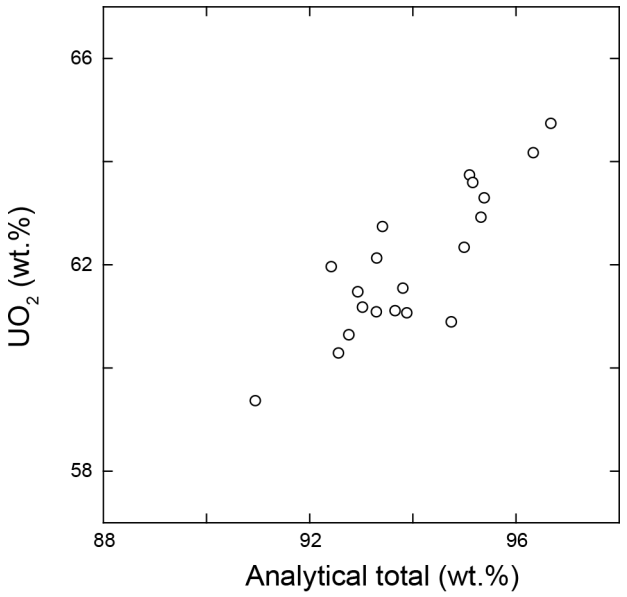

FIGURE 2 Correlation diagram of UO_2 contents and analytical totals obtained by EPMA analysis in Faraday uraninite

TABLE 2 ICP–MS results for Faraday uraninite

	$^{206}Pb/^{238}U$
1	0.1599
2	0.1610
3	0.1580
4	0.1699
5	0.1673
6	0.1622
Average	0.163
2 S.D.	0.009

Zr and Hf replacing U. Faraday uraninite is characterized by low contents of impure elements such as Si (< 0.18 wt%) and Ca (< 0.44 wt%) and slightly high REE contents. The Pb/U ratios in Faraday uraninite are homogeneous and constant at 0.1865 ±0.0008 (SD), except at spot 10. The U and Pb contents and analytical total at spot 10 are slightly lower than those at other spots (Table 1 and Figure 2). The Si content at spot 10 (SiO_2: 0.18 wt%) is higher than that at other spots (SiO_2 < 0.03 wt%), which indicates that some parts of Faraday uraninite have been altered (e.g., Finch & Ewing, 1992; Foord, Korzeb, Lichte, & Fitzpatrick, 1997; Kempe, 2003; Pearcy, Prikryl, Murphy, & Leslie, 1994). The partial alteration has resulted in Pb loss and U redistribution in Faraday uraninite. The analytical results of six fragments of the Faraday uraninite with ICP–MS also confirm the homogeneity of the Pb/U elemental ratio in the uraninite within a variation of 6% (2S.D., Table 2).

The Pb/U ratio of 0.1865 obtained from the EPMA analysis is lower than that reported previously (0.214; Robinson & Sabina, 1955). There are two possible reasons of the lower Pb/U ratio: (i) substitution of U with Th in the Faraday uraninite and (ii) younger crystallization age of the Faraday uraninite. The latter is discussed in next section. From Table 1, it is clear that Faraday uraninite used in this study contains a larger amount of Th (Th > 14.9 wt% and Th/U > 0.27) as compared to the sample analyzed by Robinson and Sabina (1955) (Th = 6.8 wt% and Th/U = 0.11). The longer half-life of Th (1.4×10^{10} year) as compared to the half-lives of U isotopes (^{235}U and ^{238}U: 7.4×10^8 and 4.47×10^9 year, respectively) slows the Pb growth in the Th rich uraninite sample, resulting low concentration of Pb and low Pb/U ratio.

4.1.2 | Pb isotopic compositions

The Pb isotopic compositions in Faraday uraninite determined from 21 spots by SHRIMP analysis are also homogeneous and constant within a variation of 0.2% in the $^{207}Pb/^{206}Pb$ and $^{208}Pb/^{206}Pb$ ratios (Table 3). The counts of the Pb hydrides $^{209}(PbH)^+$ are almost equal to the background level, thus the interference from the Pb hydrides has not been corrected in this study. As shown in Table 3, the isotopic abundance of ^{204}Pb in Faraday uraninite is negligibly low ($^{204}Pb/^{206}Pb$ < 0.000006), which indicates that Faraday uraninite contains little initial Pb.

4.1.3 | $^{206}Pb/^{238}U$ ratio

The average $^{206}Pb/^{238}U$ ratio in Faraday uraninite from six separate measurements via ICP–MS has been found to be 0.163, corresponding to 974 Ma (Table 2). However, the bulk measurement of the $^{206}Pb/^{238}U$ ratio with ICP–MS and TIMS cannot avoid the low-Pb/U domains such as spot 10, listed in Table 1. On the other hand, the combination of the analytical data of the Pb/U elemental ratios obtained by the EPMA analysis and the Pb isotopic ratios obtained by SHRIMP analysis provides the average $^{206}Pb/^{238}U$ ratio of 0.1647, which has been calculated using the following equation that is a modification of the equation obtained by Fayek et al. (2000).

$$^{206}Pb/^{238}U = \{[Pb]\{^{206}Pb/(^{204}Pb + ^{206}Pb + ^{207}Pb + ^{208}Pb)\}/\{[U]\{^{238}U/(^{235}U + ^{238}U)\}\}$$

where [Pb] and [U] are the measured concentrations of Pb and U, respectively.

The calculated $^{206}Pb/^{238}U$ ratio of 0.1647 is slightly higher than that obtained in the ICP–MS analysis (0.163), and provides age of 983 Ma. The age is consistent with the SHRIMP Pb–Pb age of 987 Ma calculated from the average $^{207}Pb/^{206}Pb$ ratio without applying the common Pb correction. Difference between the calculated $^{206}Pb/^{238}U$ age and the Pb–Pb age expressed as % discordance (defined as {1-($^{206}Pb/^{238}U$ age)/($^{207}Pb/^{206}Pb$ age)}× 100 (%)) (e.g., Song, Nutman, Dunyi, & Jiashan, 1996)) is 0.47, whereas that between the ICP–MS results and the Pb–Pb age is 1.38. The higher discordance of the ICP–MS results is attributed to inclusion of the altered domain with low Pb/U ratio.

TABLE 3 Pb isotopic compositions in Faraday uraninite measured by using SHRIMP

	$^{204}Pb/^{206}Pb$	$^{207}Pb/^{206}Pb$	$^{208}Pb/^{206}Pb$
1	0.0000017 ± 0.0000008	0.073 2 ± 0.0004	0.065 6 ± 0.0002
2	0.0000058 ± 0.0000015	0.073 3 ± 0.0006	0.069 2 ± 0.0008
3	0.0000013 ± 0.0000011	0.070 5 ± 0.0003	0.070 7 ± 0.0003
4	0.0000008 ± 0.0000008	0.071 1 ± 0.0002	0.067 3 ± 0.0002
5	0.0000019 ± 0.0000007	0.071 4 ± 0.0003	0.067 1 ± 0.0003
6	0.0000017 ± 0.0000007	0.071 5 ± 0.0002	0.070 0 ± 0.0003
7	0.0000006 ± 0.0000003	0.072 3 ± 0.0003	0.069 0 ± 0.0003
8	0.0000011 ± 0.0000010	0.073 0 ± 0.0002	0.068 3 ± 0.0003
9	0.0000015 ± 0.0000013	0.073 9 ± 0.0004	0.066 1 ± 0.0003
10	0.0000006 ± 0.0000004	0.072 7 ± 0.0003	0.067 7 ± 0.0003
11	0.0000020 ± 0.0000007	0.073 7 ± 0.0002	0.070 3 ± 0.0002
12	0.0000006 ± 0.0000007	0.071 3 ± 0.0004	0.066 9 ± 0.0004
13	0.0000003 ± 0.0000006	0.071 2 ± 0.0004	0.069 2 ± 0.0004
14	0.0000012 ± 0.0000009	0.072 3 ± 0.0014	0.069 3 ± 0.0009
15	0.0000010 ± 0.0000008	0.071 7 ± 0.0003	0.068 5 ± 0.0004
16	0.0000030 ± 0.0000015	0.072 6 ± 0.0005	0.067 5 ± 0.0007
17	0.0000037 ± 0.0000014	0.070 3 ± 0.0004	0.068 2 ± 0.0011
18	0.0000004 ± 0.0000006	0.071 6 ± 0.0004	0.069 5 ± 0.0005
19	n.d.	0.073 1 ± 0.0006	0.065 8 ± 0.0002
20	0.0000037 ± 0.0000013	0.071 4 ± 0.0003	0.068 3 ± 0.0003
21	0.0000026 ± 0.0000009	0.071 1 ± 0.0004	0.068 7 ± 0.0003
Average	0.0000017 ± 0.00000014	0.072 1 ± 0.00010	0.068 3 ± 0.00014

n.d., ^{204}Pb not detected.
All analytical uncertainties are 1σ of the mean value.

The $^{206}Pb/^{238}U$ age of 983 Ma is lower than the previous reported age of Faraday uraninite, which is 1 045 Ma ±30 Ma, determined by Pb isotopic dating (Robinson, 1960). The granitic pegmatites of the Grenville Province intruded between 1 088 and 992 Ma (Easton, 1986a, 1986b; Mezger, Essene, van der Pluijm, & Halliday, 1993). The uranium mineralization occurred in association with the intrusion of the pegmatitic pyroxene granite dykes at 1020 Ma (Rimsaite, 1982), which indicates that the crystallization age of Faraday uraninite is younger than that of the pegmatitic pyroxene granite dykes, i.e., 1 020 Ma. Though it is necessary to have precise crystallization age of the granite with SHRIMP or LA–ICP–MS on zircons. The uranium enrichment in the Faraday mine occurred in two stages: (i) primary magmatic concentration and (ii) post-magmatic alteration involving deformation, hydrothermal activity, and metasomatic reactions with the host rocks (Masson & Gordon, 1981). The secondary enrichment of uranium in pegmatite occurred due to the chemical interaction with the host rocks (Lentz, 1996). Considering previous chronological and mineralogical studies, the $^{206}Pb/^{238}U$ ratio of 0.1647 obtained by the EPMA and SHRIMP analyses is reasonable and probably reflects secondary enrichment. Therefore, in this study, the $^{206}Pb/^{238}U$ ratio of 0.1647 is used for the calibration of the SHRIMP $^{206}Pb/^{238}U$ data of uraninite.

4.1.4 | Calibration of Pb^+/U^+ to Pb/U

In order to calibrate measured Pb^+/U^+ to Pb/U, the correlation between $^{251}UO^+/^{235}U^+$ and $^{206}Pb^+/^{235}U^+$ in Faraday uraninite was carefully examined. Measurements have been carried out at 70 different analytical spots in 12 grains over a period of 3 days. Fayek, Kyser, and Riciputi (2002) have reported the inter-element fractionation between U and Pb as a function of the primary ion beam current and the dead-time correction of an electron multiplier. Black and Jagodzinski (2003) have also pointed out the correlation between the varying primary beam intensity and the dispersion from the Pb/U calibration during zircon measurement. In order to prevent the variation in the fractionation between U and Pb, the variation in the primary beam intensity was minimized. Figure 3 shows the relationship between the $^{206}Pb^+/^{235}U^+$ ratio and the $^{251}(UO)^+/^{235}U^+$ ratio in Faraday uraninite. Detailed data can be found in Table S1. Although a drift was observed in the correlation of these two ratios on a daily basis, the following empirical formula was obeyed:

$$\ln\left(^{206}Pb^+/^{235}U^+\right) = a \times \ln\left(^{251}(UO)^+/^{235}U^+\right) + b$$

where a and b are the slope (exponent) and the intercept on the y-axis, respectively, and have been found to be constant from the

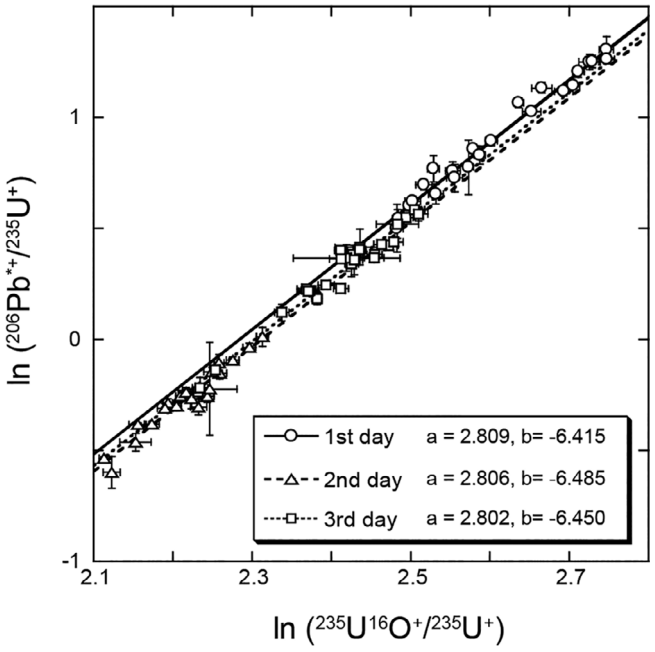

FIGURE 3 Correlation diagram of $^{206}Pb^{+}/^{235}U^{+}$ and $^{251}(UO)^{+}/^{235}U^{+}$ ratios in Faraday uraninite. a and b are the slope (exponent) and the intercept on the y-axis of the calibration curve, respectively

analyses of the reference sample. As shown in Figure 3, the slopes of each day are shifted each other during 3 days (2.809, 2.806, and 2.802, respectively), whereas the intercepts on the y-axis show a small variation (−6.415, −6.485 and −6.450, respectively). The variation suggests that the fractionation between U and Pb occurs in association with the daily differences in the primary beam condition (Fayek, Kyser, & Riciputi, 2002). The slope estimated from the all data for the three-day measurement is 2.968 and is steeper than the average slope for each day, i.e., 2.805, which indicates that the slope estimated from all data includes the variation in the y-axis, namely, the fractionation between U and Pb. Therefore, the average slope of 2.805 ±0.123 is used for the calibration of the SHRIMP data. The calibration uncertainty (4.4%), defined as the uncertainty in the slope, is higher than that in the common zircon analyses (less than 2%, e.g., Claoué-Long et al., 1995).

Figure 3 suggests that the calibration method that is similar to that used in the zircon analysis is useful for the U–Pb analysis of uraninite. However, Fayek, Kyser, and Riciputi (2002) have reported a weak correlation between $^{206}Pb^{+}/^{238}U^{+}$ and $^{254}(UO)^{+}/^{238}U^{+}$ due to the presence of impurity elements in the uraninite matrix because the differences in the contents of other elements (i.e., Si, Ca) may affect the ionization efficiencies of Pb^{+} and U^{+}. The correlation coefficients between $^{206}Pb^{+}/^{235}U^{+}$ and $^{251}(UO)^{+}/^{235}U^{+}$ in Faraday uraninite are calculated to be r = 0.989, 0.968, and 0.982 for each day, respectively, which indicates that the correlation curve can be efficiently used for the calibration of Pb^{+}/U^{+} to Pb/U. The $^{206}Pb/^{238}U$ ratios in uraninites are calculated using the following equation:

$$\left(^{206}Pb/^{238}U\right)_{unk} = \left(^{206}Pb^{+}/^{235}U^{+}\right)_{unk} / \left(^{206}Pb^{+}/^{235}U^{+}\right)_{ref} \times \left(^{206}Pb/^{238}U\right)_{ref}$$

where $(^{206}Pb^{+}/^{235}U^{+})$ and $(^{206}Pb/^{238}U)$ are the measured secondary ion ratio and the isotopic ratio, respectively. The subscripts "unk" and "ref" denote the unknown sample and the reference uraninite sample, respectively. The $^{206}Pb^{+}/^{235}U^{+}$ ratio in the unknown sample can be estimated from the calibration equation.

4.1.5 | Comparison of Pb/U ratios obtained by EPMA and SHRIMP analyses

The Pb/U calibration method was applied to three uraninite samples obtained from Chardon, Ecarpière, and Mistamisk. Previous studies have pointed out the analytical difficulties in the U–Pb analysis of uraninite because the ionization efficiencies of U^{+} and Pb^{+} in uraninite strongly depend on the matrix compositions of the uraninite sample (Fayek et al., 2000; Fayek & Kyser, 1997). Prior to the SHRIMP analysis, analytical spots were selected by BSE imaging and EPMA analysis.

Table 4 lists the U, Th, and Pb contents in the three uraninites. Tables 1 and 4 show that there are differences in the chemical compositions between the Faraday uraninite and the three uraninite samples. The U contents in Chardon, Ecarpière, and Mistamisk uraninites (more than 70.18, 66.8, and 64.03 wt%, respectively) are higher than the U content in Faraday uraninite (53.14–57.06 wt%). Faraday uraninite contains a large amount of Th (Th > 14.94 wt%), whereas Chardon and Ecarpière uraninites contain a negligible amount of Th (ThO_2 < 0.02 wt%), and Mistamisk uraninite contains a small amount of Th (ThO_2 < 0.63 wt%). Moreover, the Si and Ca contents in Chardon, Ecarpière, and Mistamisk uraninites (SiO_2 > 0.34, 0.35, and 0.03 wt%; CaO > 7.02, 8.09, and 0.68 wt%, respectively, excluding spot 1 in Mistamisk uraninite) are higher than those in Faraday uraninite (SiO_2 < 0.03 wt% and CaO < 0.3 wt%). The U–Pb data for Chardon, Ecarpière, and Mistamisk uraninites obtained from the SHRIMP analysis were carefully compared with the EPMA results to discuss the matrix effects on the U and Pb ionization efficiencies in the uraninites.

Figure 4 shows the comparison between the Pb/U ratio of the EPMA and SHRIMP analyses for Chardon, Ecarpière, and Mistamisk uraninites. Considering the time-dependent drift of the U–Pb calibration curve, shown in Figure 4, the primary beam intensity was maintained to be constant, and analyses of Faraday reference uraninite were performed after every two analysis of the uraninite samples. The SHRIMP $^{206}Pb^{*}/^{238}U$ data for the uraninites show a good correlation with the EPMA data. The correlation coefficients between the SHRIMP and EPMA data have been calculated to be r = 0.98, 0.99, and 0.97 for Chardon, Ecarpière, and Mistamisk uraninites, respectively. These values indicate that the calibration method using Faraday uraninite as a standard can provide efficient estimation of the $^{206}Pb/^{238}U$ ratios in Chardon, Ecarpière, and Mistamisk uraninites.

TABLE 4 Chemical composition of major elements and SHRIMP U–Pb data in uraninite samples

(a) Chardon uraninite									
	1	2	3	4	5	6	7	8	9
EPMA									
UO_2	79.85	79.62	79.86	80.22	80.31	79.72	79.96	80.02	79.88
ThO_2	n.d.	n.d.	n.d.	n.d.	n.d.	n.d.	n.d.	n.d.	n.d.
PbO	4.05	3.40	4.10	3.76	4.08	4.03	4.08	3.66	3.54
CaO	7.36	7.35	7.30	7.09	7.28	7.11	7.31	7.02	7.13
SiO_2	1.14	0.82	1.02	0.94	0.34	0.62	0.82	1.03	0.99
Ce_2O_3	n.d.	0.13	n.d.	0.04	0.64	0.57	0.63	0.69	0.11
Y_2O_3	0.03	0.01	0.05	n.d.	1.35	1.32	1.41	1.29	0.04
Na_2O	0.67	0.56	0.60	0.59	0.02	0.10	0.02	0.06	0.54
F	1.39	1.38	1.40	1.34	0.04	0.01	0.06	0.02	0.44
Total	94.49	93.28	94.32	93.98	94.06	93.49	94.28	93.79	92.67
SHRIMP									
U	70.39	70.18	70.40	70.71	70.79	70.27	70.48	70.54	70.41
Pb	3.76	3.16	3.81	3.49	3.79	3.74	3.79	3.40	3.29
Pb/U	0.0534	0.0450	0.0541	0.0494	0.0535	0.0532	0.0537	0.0482	0.0467
$^{206}Pb^*/^{238}U$	0.0501	0.0412	0.0513	0.0481	0.0501	0.0500	0.0504	0.0443	0.0435
1σ	0.0020	0.0064	0.0014	0.0033	0.0016	0.0019	0.0023	0.0022	0.0047
(b) Ecarpière uraninite									
	1	2	3	4	5	6	7	8	9
EPMA									
UO_2	78.91	78.81	79.59	79.23	79.35	79.66	79.78	77.78	75.78
ThO_2	n.d.	n.d.	0.02	n.d.	n.d.	n.d.	n.d.	n.d.	n.d.
PbO	3.34	3.33	3.44	3.34	3.59	3.43	3.46	2.86	2.41
CaO	8.33	8.10	8.18	8.39	8.94	8.09	9.51	9.95	8.79
SiO_2	0.35	0.87	0.38	0.39	0.55	0.94	0.45	3.55	5.45
Ce_2O_3	0.07	0.23	0.20	0.19	0.16	0.14	0.20	0.10	0.13
Y_2O_3	0.10	0.17	0.15	0.14	0.11	0.11	0.06	0.05	0.04
Na_2O	0.64	0.62	0.66	0.66	0.39	0.56	0.65	0.25	0.35
F	2.24	2.07	2.14	2.46	1.80	1.78	2.51	0.32	0.51
Total	93.98	94.20	94.76	94.80	94.87	94.71	96.62	94.86	93.46
SHRIMP									
U	69.56	69.47	70.16	69.84	69.95	70.22	70.33	68.56	66.80
Pb	3.10	3.09	3.19	3.10	3.33	3.18	3.21	2.65	2.24
Pb/U	0.0446	0.0445	0.0455	0.0444	0.0476	0.0453	0.0457	0.0387	0.0335
$^{206}Pb^*/^{238}U$	0.0448	0.0449	0.0453	0.0448	0.0474	0.0458	0.0459	0.0386	0.0354
1σ	0.0034	0.0017	0.0028	0.0027	0.0034	0.0029	0.0029	0.0046	0.0029
(c) Mistamisk uraninite									
	1	2	3	4	5	6	7	8	
EPMA									
UO_2	72.79	75.62	75.88	72.64	76.76	74.28	72.98	75.28	
ThO_2	0.63	n.d.	n.d.	n.d.	0.05	0.12	0.01	n.d.	
PbO	18.27	16.15	15.19	14.23	11.28	20.34	17.53	17.22	
CaO	0.17	2.12	2.41	1.53	2.67	0.68	2.51	1.34	

(Continues)

TABLE 4 (Continued)

(c) Mistamisk uraninite								
	1	2	3	4	5	6	7	8
SiO_2	0.03	0.48	0.27	0.09	0.12	0.04	0.19	0.35
Ce_2O_3	0.17	0.54	0.46	0.43	0.39	0.11	0.46	0.45
Nd_2O_3	0.04	0.44	0.48	0.45	0.42	0.04	0.49	0.32
Sm_2O_3	0.13	0.09	0.20	0.10	0.15	0.12	0.14	0.10
Yb_2O_3	0.03	0.09	0.16	0.06	0.09	0.04	0.06	0.07
Er_2O_3	n.d.	0.09	0.14	0.02	0.12	n.d.	0.09	0.10
Dy_2O_3	0.18	0.35	0.42	0.23	0.37	0.16	0.21	0.37
Gd_2O_3	0.10	0.10	0.33	0.36	0.30	0.09	0.31	0.21
Y_2O_3	0.25	0.67	0.94	0.78	0.77	0.20	0.86	0.77
Total	92.77	96.74	96.88	90.91	93.47	96.22	96.58	96.58
SHRIMP								
U	64.16	66.66	66.89	64.03	67.66	65.48	64.33	66.36
Pb	16.96	14.99	14.10	13.21	10.47	18.88	16.27	15.99
Pb/U	0.2643	0.2249	0.2109	0.2062	0.1547	0.2884	0.2530	0.2409
$^{206}Pb^*/^{238}U$	0.268	0.222	0.209	0.183	0.163	0.291	0.258	0.247
1σ	0.017	0.042	0.037	0.005	0.021	0.040	0.046	0.016

n.d., not detected.
All EPMA data in wt%.

4.2 | U–Pb dating of uraninite samples

4.2.1 | Internal textures and chemical composition of uraninites

Kempe (2003) has suggested that the internal textures and the variation in the Si and Ca contents are useful criteria for studying the alteration phases in uraninite. The BSE images of the uraninite samples are shown in Figure 5. Chardon uraninite, which is Ca-rich uraninite (CaO > 7.02 wt%), contains a large number of micro inclusions such as marcasite (FeS_2), goethite (FeOOH), and Pb oxide (Figure 5a) which have been identified from SEM-EDS and micro-Raman spectroscopy. Ecapière uraninites are associated with Fe-sulfides (Cathelineau, 1981), but the EDS analysis could not detect the presence of Fe and S in them. The Pb/U ratios obtained from the EPMA analyses are scattered in the range of 0.0 450 to 0.0 541, which suggests that U–Pb systems in some parts of Chardon uraninite have been disturbed. Kempe (2003) has reported a correlation between the Pb/U ratios and the Si and Ca contents in uraninite altered by fluids. Chardon uraninite does not show such a correlation, which suggests that Chardon uraninite originally contains Ca and Si. The variation in the Pb/U ratios in Chardon uraninite is probably due to the partial Pb loss such as thermal diffusion, which is supported by larger deviation of Pb contents (standard deviation: 0.25) than those of U (0.19).

Ecarpière uraninite, which is also Ca-rich uraninite (CaO > 8.09 wt %), shows homogeneous chemical composition except 5–10 μm around fractures characterized by darker brightness of BSE response (Figure 5b). Table 4 shows that the Pb/U ratios are constant (0.0 454 ±0.0 011), except Nos. 8 and 9 which are dark domains around fractures (0.0 387 and 0.0 335, respectively). The Si contents in the dark domains (SiO_2: 3.55 and 5.45 wt%, respectively) are higher than those in the bright domains (SiO_2 < 0.94 wt%), whereas the U contents in the dark domains (U: 68.56 and 66.80 wt%, respectively) are lower than those in the bright domains (U > 69.47 wt%), which indicates that the vicinity of the fractures in Ecarpière uraninite has been altered. Figure 6 shows a correlation between the UO_2 contents and the analytical totals. Except for the low Pb/U spots (Chardon: spots 2, 8, and 9; Ecarpière: 8 and 9), the UO_2 contents show a correlation with the analytical totals, which indicates that low analytical totals in Chardon and Ecarpière uraninites (92.67–94.49 and 93.46–96.62 wt %, respectively) may be caused by the presence of unanalyzed elements replacing U.

Mistamisk uraninite shows a patchy texture (Figure 5c). The patchy texture of Mistamisk uraninite indicates that some parts of the sample has been affected by alteration (Kempe, 2003). Table 4 shows a variation in the Pb/U ratios (0.1547–0.2884) and the contents of Th (ThO_2: < 0.63 wt%), CaO (0.17–2.67 wt%) and SiO_2 (0.03–0.48 wt%). As shown in Figure 7, the correlation between the Pb/U ratios and the Ca contents suggests that U–Pb system has been disturbed by an alteration event (Kempe, 2003).

4.2.2 | Chronological interpretation

Figures 8 and 9 show the U–Pb isotopic data for Ecarpière, Mistamisk, and Chardon uraninite, respectively. The analytical uncertainties in the $^{238}U/^{206}Pb^*$ ratios are higher than those in the $^{207}Pb^*/^{206}Pb^*$ ratios due to the large calibration uncertainty.

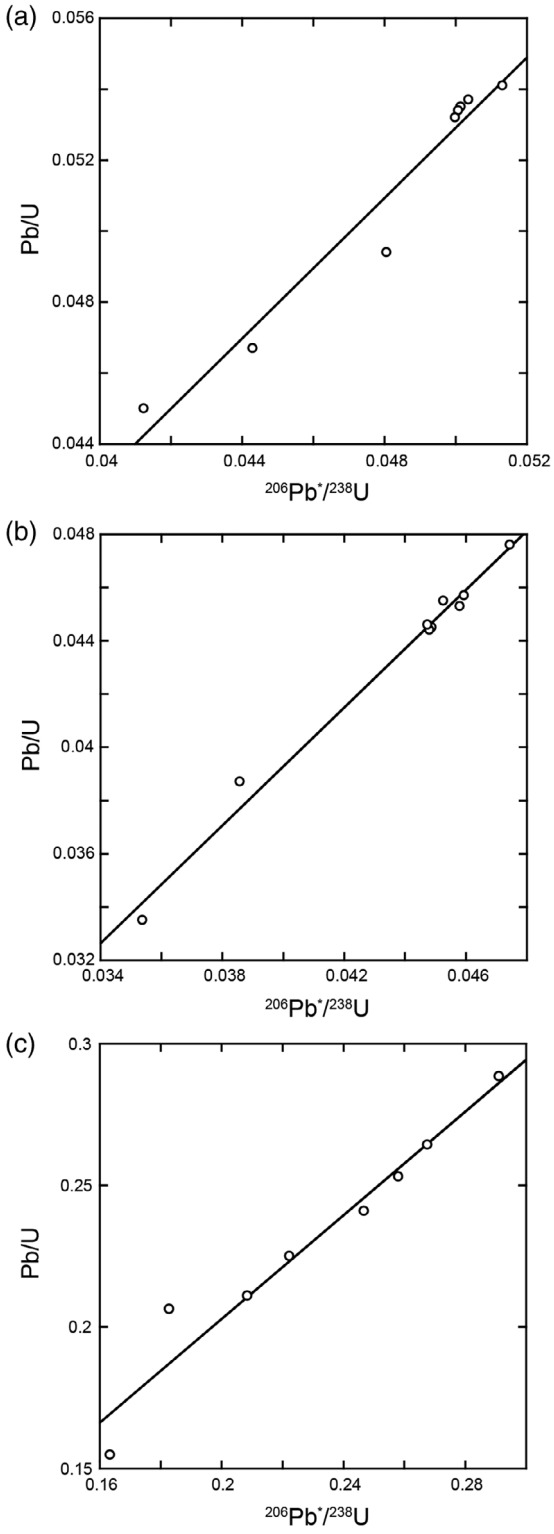

FIGURE 4 Comparison of the Pb/U ratios obtained from EPMA analysis and $^{206}Pb^{*}/^{238}U$ ratios obtained from SHRIMP analysis for (a) Chardon, (b) Ecarpière, and (c) Mistamisk uraninites

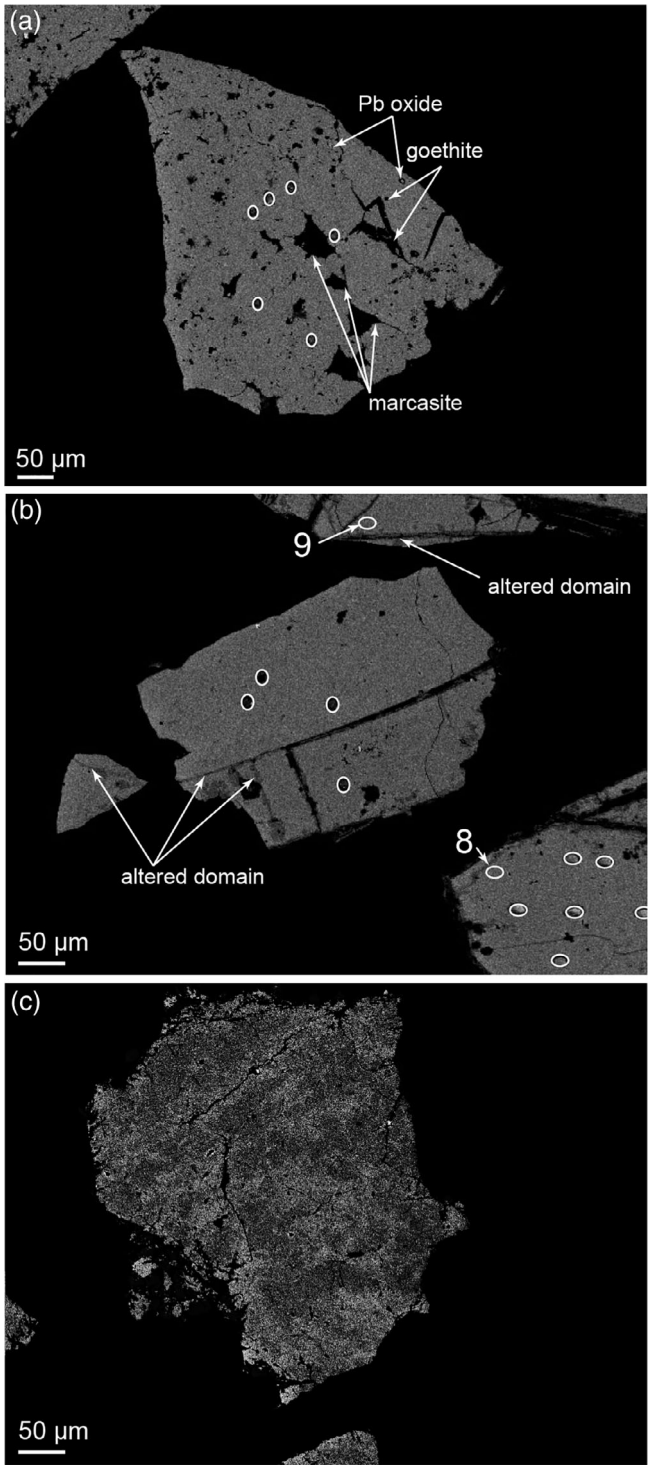

FIGURE 5 BSE images of (a) Chardon uraninite containing a large number of micro inclusions such as marcasite (FeS_2), goethite (FeOOH), and Pb oxide, (b) Ecarpière uraninite showing darker brightness domain of BSE response at 5–10 μm around vicinity of fractures, and (c) Mistamisk uraninite showing patchy texture. White circles show SHRIMP spots including the spots which are not associated with this work. Spot number is in common with Table 4

4.2.3 | Ecarpière uraninite

Cathelineau et al. (1990) have reported that Ecarpière uraninite has remarkably homogeneous U and Pb contents over large areas (> 200 μm). We have also confirmed from the BSE images and the chemical composition data that Ecarpière uraninite shows homogeneous Pb/U ratios except 5–10 μm around fractures characterized by

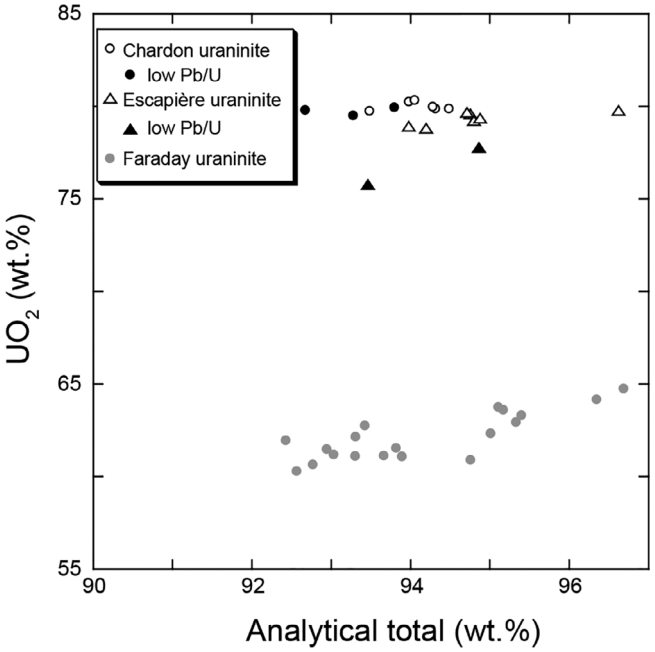

FIGURE 6 Correlation diagram of UO_2 contents and analytical totals obtained by EPMA in Chardon and Ecarpière uraninite plotted with data of Faraday uraninite

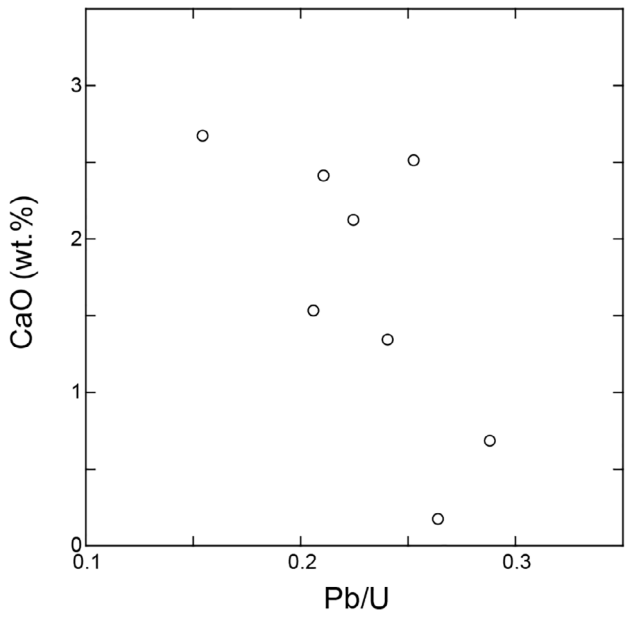

FIGURE 7 Correlation diagram of Pb/U ratio and Ca content in Mistamisk uraninite

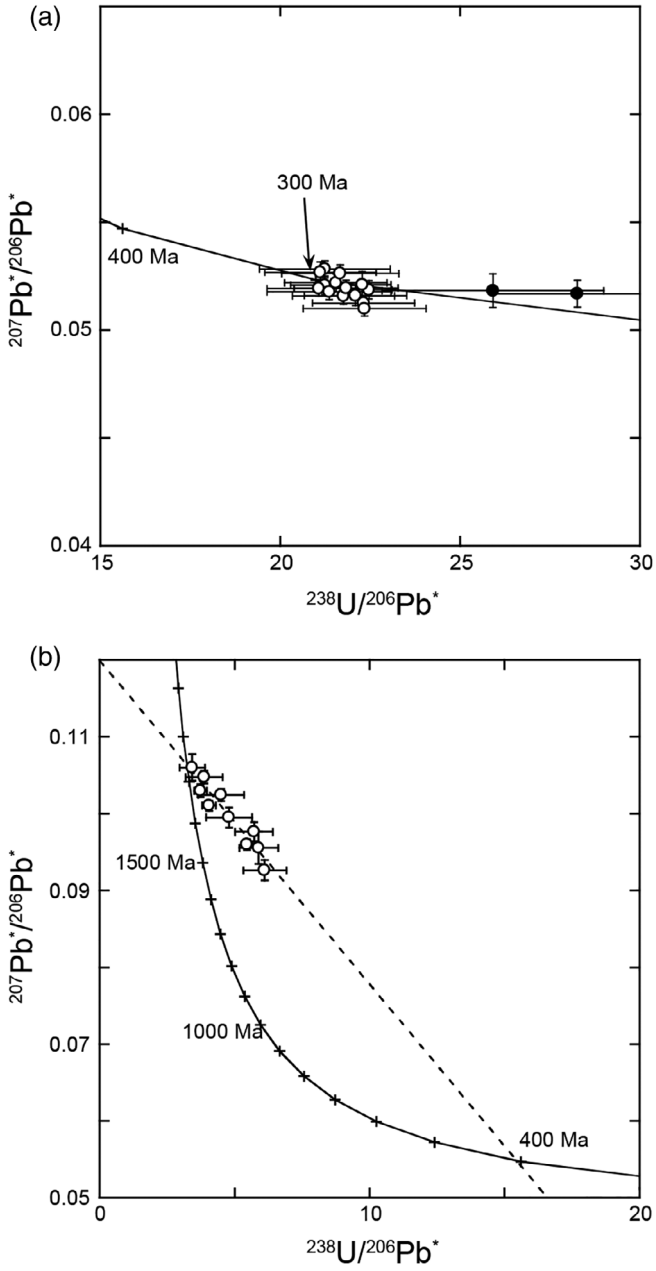

FIGURE 8 Tera-Wasserburg concordia diagrams for (a) Ecarpière and (b) Mistamisk uraninites. The filled circles indicate data rejected in the age calculation. The uncertainties are 1σ of the mean values

darker brightness of BSE response (Figure 5b and Table 4). The U–Pb analyses of the homogeneous Pb/U phases of Ecarpière uraninite provide concordant U–Pb data (Figure 8a). The U–Pb age of Ecarpière uraninite is 287 Ma ±8 Ma (95% conf.) and is consistent with the previous chronological results of fibroradial pitchblende and pitchblende with hematite (286 Ma ±7 Ma; Cathelineau et al., 1990). Therefore, the U–Pb age found in our study, i.e., 287 Ma ±8 Ma, supports the previous mineralization history, in which major U deposition along the northern contact fault of Mortagne granite occurred in association with the tectonic reactivation of the South Armorican Shear Zone during 290 Ma–270 Ma (Cathelineau et al., 1990).

On the other hand, the U–Pb analyses of the dark domains observed in the BSE image, such as Nos. 8 and 9 provide discordant U–Pb data. The EPMA data of the two spots also show low Pb/U ratios and U and Pb contents (Table 4). On the basis of the high Si contents (Table 4), it can be assumed that the remobilization of U and Pb has occurred in the dark domains during the alteration. The result of U–Pb dating in this study supporting the previous mineralization history suggests that our calibration method using Faraday uraninite except the dark domains in the BSE images is useful for a Ca-rich uraninite.

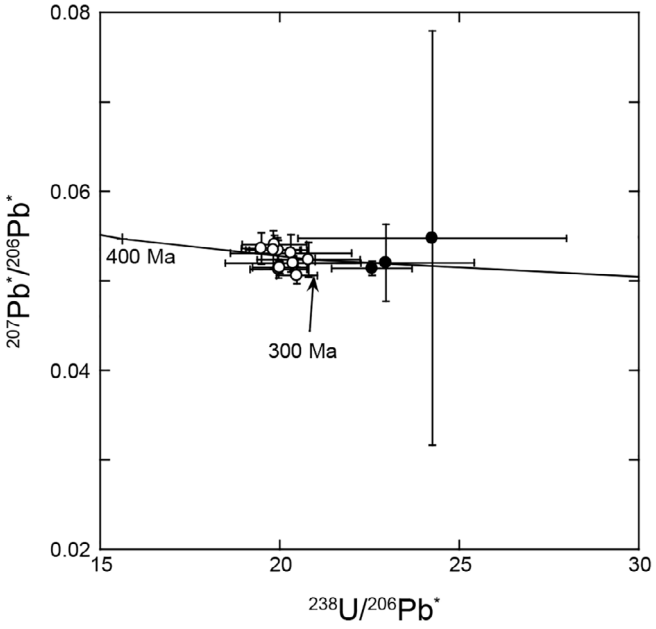

FIGURE 9 Tera-Wasserburg concordia diagram for Chardon uraninite. The filled circles indicate data rejected in the age calculation. The uncertainties are 1σ of the mean values

4.2.4 | Mistamisk uraninite-albite veins

Bonhoure, Kister, Cuney, and Deloule (2007) and Takahashi et al. (2002) have reported that Mistamisk uraninite shows homogeneous distributions of REE over the grains. The BSE image of Mistamisk uraninite shows a patchy texture indicating heterogeneous chemical compositions (Figure 5c). In Figure 7, the dark domain observed in the BSE image is characterized by higher Ca contents and lower Pb/U ratios as compared to the bright domain. The patchy texture and the scattered Pb/U ratios (0.1 547–0.2 884) in Mistamisk uraninite suggest that the U–Pb system has been disturbed by the alteration event due to its low crystallinity caused by the radiation damages. The U–Pb isotopic analyses of Mistamisk uraninite also show a disturbance in the U–Pb system (Figure 8b). The calculations and regressions of discordant U–Pb data are after Davis (1982). The upper intercept age of 1 729 Ma ±40 Ma is consistent with previous chronological reports based on TIMS (ca. 1 800 Ma; Kish & Cuney, 1981) and SIMS (1 724 Ma ±7 Ma corresponding to the Hudsonian orogeny event; Holliger, 1988). As shown in Table 4, the correlation between the $^{206}Pb^*/^{238}U$ ratios and the Pb contents indicates Pb loss in some parts of the uraninite. The lower intercept age of 421 Ma ±98 Ma corresponds to a period of high orogenic activity in North America (e.g., the Taconic and Acadian orogenies), which suggests that the Pb loss has occurred during the remobilization of U in association with the thermal event.

The results for Ecarpière and Mistamisk uraninites are consistent with previously reported chronological results, which indicates that the established calibration method using Faraday uraninite is useful.

4.2.5 | Chardon uraninite

Because Chardon uraninite contains several types of micro inclusions (Figure 5a), the U–Pb isotopic analyses of Chardon uraninite sample were carried out after a careful selection of the analytical spots in order to avoid such impure phases. Figure 9 shows a U–Pb concordia diagram for Chardon uraninite. The $^{206}Pb^*/^{238}U$ ratios (0.0412–0.043) at three analytical spots are lower than the other 11 spots (0.0481–0.0513). The EPMA data for the three spots also show low Pb contents (Nos. 2, 8, and 9 in Table 4). The U–Pb age of the Chardon uraninite, excluding the data from the spots with low Pb contents, is calculated to be 315 Ma ±7 Ma (95% conf.). This age is consistent with the intrusion age of the Mortagne granite of 310 Ma ±10 Ma (Sonet, 1967) and 313 Ma ±5 Ma (Guineberteau, 1986), but older than that obtained from the previous chronological result (264 Ma ±9 Ma; Cathelineau et al., 1990). Previous studies have reported that the uranium mineralization in the Chardon mine occurred in association with the hydrothermal activity during the cooling of the Mortagne granite (Cathelineau, 1981; Cathelineau et al., 1990; Cathelineau & Leroy, 1981; Lillié, 1974). From the mineralogical observation of the sample, it is evident that goethite was formed from marcasite under an oxidizing condition (Rinker, Nesbitt, & Pratt, 1997; Wiersma & Rimstidt, 1984). Under the oxidizing condition, uranium is mobilized as UO_2^{2+}. Moreover, all U–Pb data obtained by Cathelineau et al. (1990) by combining the data of TIMS and SIMS analyses are discordant, which suggests that the U–Pb system in Chardon uraninite has been partially disturbed after mineralization. Therefore, it is reasonable that some parts of Chardon uraninite were crystallized by the igneous activity of Mortagne granite, and then the uranium ore body was formed by the hydrothermal activity. After the formation of the ore body, the uraninite released Pb under the oxidizing condition.

4.3 | Advantage of the established calibration method

The results of U–Pb isotopic analyses of Ecarpière and Mistamisk uraninites using the established calibration method, which is similar to the calibration method used in conventional zircon analysis, are consistent with those obtained in previous chronological studies. In addition, the U–Pb data of Chardon uraninite provide a new insight into ore formation. These results indicate that the established calibration method using the Faraday uraninite is useful for isotopic dating on the scale of a few micrometers to tens of micrometers, which makes it possible to discuss exact and detailed age of uraninite. The application of this method enables us to eliminate the use of a combination of EPMA and SIMS analyses, thereby reducing the efforts involved. On the other hand, the age obtained using the RSF approach can differ from the actual age by more than an order of magnitude depending on the analytical conditions and the instrument used (Homma, 1994; Simons et al., 1990; Williams, 1998). As a result, different instruments cannot be used when this method is used. Because the established calibration method is independent of instruments as well as that of zircon, this method can be employed by using various types of SIMS instruments.

5 | CONCLUSIONS

A method for the U–Pb isotopic analysis of uraninite using SHRIMP has been established. The relationship between $^{251}(UO)^{+}/^{235}U^{+}$ and $^{206}Pb^{+}/^{235}U^{+}$ is useful for the calibration from ion ratios to atomic abundance ratios. The EPMA, ICP–MS, and SHRIMP analyses of Faraday mine uraninite show that it has the sufficiently homogeneous Pb/U ratio and the Pb isotopic composition (average $^{206}Pb/^{238}U$ ratio of 0.1 647) as the reference material for the U–Pb analysis by SIMS.

The established calibration method has been applied to three uraninite samples collected from Chardon, Ecarpière, and Mistamisk mines. The results of the U–Pb analyses of Ecarpière uraninite (287 Ma ±8 Ma) and the Mistamisk uraninite-albite veins (the upper intercept age of 1 729 Ma ±40 Ma) show good consistency with those obtained in previous chronological studies (286 Ma ±7 Ma and 1 724 Ma ±7 Ma, respectively). The consistency of results for Ecarpière and Mistamisk uraninites indicate that the established calibration method using Faraday uraninite is useful for the analysis of uraninite. The U–Pb age of Chardon uraninite (315 Ma ±7 Ma) is consistent with the igneous activity of Mortagne granite, but is higher than the previously reported age (264 Ma ±9 Ma). The U–Pb result suggests that Chardon uraninite was formed by the hydrothermal activity during the cooling of Mortagne granite, and then uraninite released Pb under the oxidizing condition, which is a new insight into ore formation.

The established analytical method using Faraday uraninite is useful for isotopic dating on the scale of a few micrometers to tens of micrometers, which make it possible to discuss exact and detailed age of uraninite. The method allows us to determine accurate U–Pb age of uraninite with more simple way than that of a combination of Pb/U elemental ratio by EPMA analysis and Pb isotope ratio by SIMS analyses.

ACKNOWLEDGEMENTS

We are grateful to Y. Takahashi, Y. Shibata, and Y. Tsutsumi for their technical help with the ICP–MS and EPMA analyses. Faraday uraninite was donated by K. Jensen. The uraninite samples from Chardon, Ecarpière, and Mistamisk were provided by P. Holliger. We appreciate M. Ogasawara, an anonymous reviewer and M. Ikehara for constructive reviews. We would like to thank M. Takehara for the support of revising the manuscript.

This study was partly supported by a Grant-in-Aid for JSPS Fellows (to K.H., Nos. 05203 and 06290) and a Grant-in-Aid for Scientific Research (to H.H., No. 17204051) from the Japan Society for the Promotion of Science (JSPS).

ORCID

Kenji Horie https://orcid.org/0000-0001-9511-1501

REFERENCES

Bekker, A., Holland, H. D., Wang, P. -L., Rumble, D., III, Stein, H. J., Hannah, J. L., … Beukes, N. J. (2004). Dating the rise of atmospheric oxygen. *Nature*, *427*, 117–120.

Bernard-Griffiths, J., Peucat, J. J., Sheppard, S. M. F., & Vidal, P. (1985). Petrogenesis of leucogranites from the Southern Armorican Massif: Contribution of REE and isotopic (Sr, Nd, Pb and O) geochemical data to the study of source rock characteristics and age. *Earth and Planetary Science Letters*, *74*, 235–250.

Black, L. P., & Jagodzinski, E. A. (2003). Importance of establishing sources of uncertainty for the derivation of reliable SHRIMP ages. *Australian Journal of Earth Sciences*, *50*, 503–512.

Bonhoure, J., Kister, P., Cuney, M., & Deloule, E. (2007). Methodology for rare earth element determinations of uranium oxides by ion microprobe. *Geostandards and Geoanalytical Research*, *31*, 209–225.

Bowles, J. F. W. (1990). Age dating of individual grains of uraninite in rocks from electron microprobe analyses. *Chemical Geology*, *83*, 47–53.

Brandt, S. B., & Pershinov, A. V. (1968). The P-T relationships for the migration capacity of lead under hydrothermal conditions. *Geochemistry International*, *6*, 72–77.

Braun, I., Montel, J. M., & Nicollet, C. (1998). Electron microprobe dating of monazite from high-grade gneisses and pegmatites of the Kerala Khondalite Belt, south India. *Chemical Geology*, *146*, 65–85.

Cathelineau, M. (1981). Les gisements uranifères de la presqu'île Guérandaise (Sud Bretagne); approche structurale et métallogénique. *Mineralium Deposita*, *16*, 227–240.

Cathelineau, M., Boiron, M. -C., Holliger, P., & Poty, B. (1990). Metallogenesis of the French part of the Variscan orogene. Part II: Time-space relationships between U, Au and Sn-W ore deposition and geodynamic events - mineralogical and U-Pb data. *Tectonophysics*, *177*, 59–79.

Cathelineau, M., & Leroy, J. (1981). Reactions between uranium veins and their host rocks in Vendée and Limousin (France). *Mineralogical Magazine*, *44*, 417–423.

Claoué-Long, J. C., Compston, W., Roberts, J., & Fanning, C. M. (1995). Two Carboniferous ages: A comparison of SHRIMP zircon dating with conventional zircon ages and $^{40}Ar/^{39}Ar$ analysis. In W. A. Berggren, D. V. Kent, M.-P. Aubrey, & J. Hardenbol (Eds.), *Geochronology Time Scales and Global Stratigraphic Correlation*. Tulsa, OK: SEPM (Society for Sedimentary Geology) Special Publication, vol. 54.

Cocherie, A., & Albarede, F. (2001). An improved U-Th-Pb age calculation for electron microprobe dating of monazite. *Geochimica et Cosmochimica Acta*, *65*, 4509–4522.

Cocherie, A., Legendre, O., Peucat, J. J., & Kouamelan, A. N. (1998). Geochronology of polygenetic monazites constrained by in situ electron microprobe Th-U-total lead determination: Implications for lead behaviour in monazite. *Geochimica et Cosmochimica Acta*, *62*, 2475–2497.

Compston, W., Williams, I. S., & Meyer, C. E. (1984). U-Pb geochronology of zircons from lunar breccia 73217 using a sensitive high-mass resolution ion microprobe. *Journal of Geophysical Research, B*, *89*, 525–534.

Cumming, G. L., & Richards, J. R. (1975). Ore lead isotope ratios in a continuously changing earth. *Earth and Planetary Science Letters*, *28*, 155–171.

Davis, D. W. (1982). Optimum linear regression and error estimation applied to U-Pb data. *Canadian Journal of Earth Sciences*, *19*, 2141–2149.

DeWolf, C. P., Belshaw, N., & O'Nions, R. K. (1993). A metamorphic history from micron-scale $^{207}Pb/^{206}Pb$ chronometry of Archean monazite. *Earth and Planetary Science Letters*, *120*, 207–220.

Dimroth, E. (1978). Region de la Fosse du Labrador (54°30′-56°30′): Ministere des Ressources naturelles, Quebec, *Rapport Geologic*, 193, 396.

Easton, R. M. (1986a). Geochronology compilation series: Ontario Geological Survey, Open File Report 5592 with Maps P.2840–2814. Compilation Series Preliminary Map, Scale 1:1,013,760.

Easton, R. M. (1986b). Geochronology of the Grenville Province. In J. M. Moore, A. Davidson, & A. J. Baer (Eds.), The Grenville Province: Geological Association of Canada Special Paper 31 (pp. 127–174).

Evins, Z. L., Sunde, T., Schöberg, H. & Fayek, M. (2001). U and Pb isotope calibration of uraninite and galena standards for SIMS. SKB Technical Report TR-01-35.

Fayek, M., Harrison, T. M., Ewing, R. C., Grove, M., & Coath, C. D. (2002). O and Pb isotopic analyses of uranium minerals by ion microprobe and U-Pb ages from the Cigar Lake deposit. *Chemical Geology*, *185*, 205–225.

Fayek, M., Harrison, T. M., Grove, M., & Coath, C. D. (2000). A rapid in situ method for determining the ages of uranium oxide minerals: Evolution of the Cigar Lake Deposit, Athabasca Basin. *International Geology Review*, *42*, 163–171.

Fayek, M., & Kyser, K. T. (1997). Characterization of multiple fluid events and rare-earth-element mobility associated with formation of unconformity-type uranium deposits in the Athabasca Basin, Saskatchewan. *The Canadian Mineralogist*, *35*, 627–658.

Fayek, M., Kyser, K. T., & Riciputi, L. R. (2002). U and Pb isotope analysis of uranium minerals by ion microprobe and the geochronology of the McArthur River and Sue Zone uranium deposits, Saskatchewan, Canada. *The Canadian Mineralogist*, *40*, 1553–1569.

Finch, R. J., & Ewing, R. C. (1992). The corrosion of uraninite under oxidizing conditions. *Journal of Nuclear Materials*, *190*, 133–156.

Foord, E. E., Korzeb, S. L., Lichte, F. E., & Fitzpatrick, J. J. (1997). Additional studies on mixed uranyl oxide-hydroxide hydrate alteration products of uraninite from the Palermo and Ruggles granitic pegmatites, Grafton country, New Hampshire. *The Canadian Mineralogist*, *35*, 145–151.

Förster, B. & Haack, U. (1996). Multistage evolution of the Aue-Niederschlema uranium vein deposit (Erzgebirge, Germany): Evidence from pitchblende dating. Journal of Conference Abstracts, 1, 173.

Förster, H. J. (1999). The chemical composition of uraninite in Variscan granites of the Erzgebirge, Germany. *Mineralogical Magazine*, *63*, 239–252.

Fourel, F., Lancelot, J. R., Allegre, C. J., & Dupre, B. (1988). Isotopic analyses of uraniferous minerals by both U-Pb and Sm-Nd methods. *Chemical Geology*, *70*, 134 (abstract.).

Guineberteau, B. (1986). Le massif granitique de Mortagne sur Sèvre (Vendée). Structure, gravimetrie, mise en place, distribution de U-Th-K. Mémoires du Centre de Recherches sur la Géologie de l'Uranium (Nancy, France) 11, 218 (in French).

Hidaka, H., Horie, K., & Gauthier-Lafaye, F. (2007). Transport and selective uptake of radium into natural clay minerals. *Earth and Planetary Science Letters*, *264*, 167–176.

Holland, H. D. (1984). *The chemical evolution of the atmosphere and oceans*. Princeton, NJ: Princeton University Press.

Holland, H. D. (1999). When did the Earth's atmosphere become oxic? A reply. *Geochemical News*, *100*, 20–22.

Holliger, P. (1988). Ages U-Pb définis in-situ sur oxydes d'uranium à l'analyseur ionique: méthodologie et conséquences géochimiques. *Comptes Rendus de l'Académie des Sciences*, *307*, 367–373.

Holliger, P. (1992). SIMS isotope analysis of U and Pb in uranium oxides: Geological and nuclear applications. Proceedings of the 8th International SIMS Conference 719–722.

Holliger, P. (1994). Terme source: Caractérisation isotopique, paramètres nucléaires et modélisation. CCE Report FI12W-CT91-0071. Prog. Oklo-Analogues Naturels.

Holliger, P., & Cathelineau, M. (1986). Le chronomètre U-Pb en milieu uranifère: application aux gisements hydrothermaux d'uranium liés spatialement au batholite de Mortagne (Vendée, France). *Chronique de la Recherche Minière*, *485*, 33–44.

Holliger, P., & Cathelineau, M. (1987). Ion-microprobe lead isotopic measurements on U-ore minerals: Application for in-situ determined Pb-Pb apparent ages. *Terra Cognita*, *7*, 230.

Holliger, P., & Cathelineau, M. (1988). In situ U-Pb age determination by secondary ion mass spectrometry. *Chemical Geology*, *70*, 173 (abstract).

Holmes, A. (1911). The association of lead with uranium in rock-minerals, and its application to the measurement of geological time. Proceedings of the Royal Society Series A 85, No. 578, 248–256.

Homma, Y. (1994). SIMS quantitative analysis using relative sensitivity factors. Proceedings of the 9th International SIMS Conference, 135-139.

Horie, H., & Hidaka, H. (2004). Redistribution of U, Pb and REE in association with alteration of uranium minerals from the Koongarra deposit, Northern Territory, Australia. *Radiochimica Acta*, *92*, 805–808.

Horie, K., Hidaka, H., & Gauthier-Lafaye, F. (2004). Isotopic evidence for trapped fissiogenic REE and nucleogenic Pu in apatite and Pb evolution at the Oklo natural reactor. *Geochimica et Cosmochimica Acta*, *68*, 115–125.

Horie, K., Hidaka, H., & Gauthier-Lafaye, F. (2006). Elemental distribution in zircon: Alteration and radiation-damage effects. *Physics and Chemistry of the Earth*, *31*, 587–592.

Horie, K., Hidaka, H., & Gauthier-Lafaye, F. (2008). Elemental distribution in apatite, titanite and zircon during hydrothermal alteration: Durability of immobilization mineral phases for actinides. *Physics and Chemistry of the Earth*, *33*, 962–968.

Janeczek, J., & Ewing, R. C. (1995). Mechanisms of lead release from uraninite in natural fission reactors in Gabon. *Geochimica et Cosmochimica Acta*, *59*, 1917–1931.

Kempe, U. (2003). Precise electron microprobe age determination in altered uraninite: Consequences on the intrusion age and the metallogenic significance of the Kirchberg granite (Erzgebirge, Germany). *Contributions to Mineralogy and Petrology*, *145*, 107–118.

Kinny, P. D., McNaughton, N. J., Fanning, C. M. & Maas, R. (1994). 518 Ma sphene (titanite) from the Khan pegmatite, Namibia, southwest Africa: A potential ion-microprobe standard (abstract). ICOG8, Berkeley, US Geological Survey Circular 1107, 171.

Kish, L., & Cuney, M. (1981). Uraninite-albite veins from the Mistamisk Valley of the Labrador trough, Quebec. *Mineralogical Magazine*, *44*, 471–483.

Kotzer, T. G., & Kyser, T. K. (1993). O, U, and Pb isotopic and chemical variations in uraninite: Implications for determining the temporal and fluid history of ancient terrains. *American Mineralogist*, *78*, 1262–1274.

Langmuir, D. (1978). Uranium solution-mineral equilibria at low temperatures with applications to sedimentary ore deposits. *Geochimica et Cosmochimica Acta*, *42*, 547–569.

Leng, A. H., Griffith, J. W., & Steacy, H. R. (1962). Faraday mine. In R. Duhamel (Ed.), *Canadian deposits of uranium and thorium Economic Geology Series 16* (pp. 182–184). Ottawa, Canada: Geological Survey of Canada.

Lentz, D. (1996). U, Mo, and REE mineralization in late-tectonic granitic pegmatites, southwestern Grenville Province, Canada. *Ore Geology Reviews*, *11*, 197–227.

Lillié, F. (1974). Analyse tectonique et fracturation des gisements uranifères de Vendée (Thesis). Strasbourg: University of Louis Pasteur.

Ludwig, K. R. (2003). Isoplot 3.00: Berkeley Geochronology Center Special Publication 4.

Masson, S. L., & Gordon, J. B. (1981). Radioactive mineral deposits of the Pembroke-Renfrew area. *Ontario Geological Survey, Mineral Deposits Circular*, *23*, 1–155.

Meddaugh, W. S. (1983). Age and origin of uraninite in the Elliot Lake, Ontario Uranium Ores. (PhD Thesis). Cambridge, MA: Harvard University.

Mezger, K., Essene, E. J., van der Pluijm, B. A., & Halliday, A. N. (1993). U-Pb geochronology of the Grenville orogen of Ontario and New York:

Constraints on ancient crustal tectonics. *Contributions to Mineralogy and Petrology*, *114*, 13–26.

Montel, J. M., Foret, S., Veschambre, M., Nicollet, C., & Provost, A. (1996). Electron microprobe dating of monazite. *Chemical Geology*, *131*, 37–53.

Montel, J. M., Veschambre, M., & Nicollet, C. (1994). Datation de la monazite à la microsonde électronique. *Comptes Rendus de l'Académie des Sciences*, *318*, 1489–1495.

Parslow, G. R. (1982). *Chemical ages as indicators of regional uranium potential*. Proceedings of IAEA Symposium on Uranium Exploration Methods, IAEA, Vienna, pp 209–216.

Pearcy, E. C., Prikryl, J. D., Murphy, W. M., & Leslie, B. W. (1994). Alteration of uraninite from the Nopal I deposit, Peña Blanca District, Chihuahua, Mexico, compared to degradation of spent nuclear fuel in the proposed U.S. high-level nuclear waste repository at Yucca Mountain, Nevada. *Appied Geochemistry*, *9*, 713–732.

Peng, G., Luhr, J. F., & McGee, J. J. (1997). Factors controlling sulfur concentrations in volcanic apatite. *American Mineralogist*, *82*, 1210–1224.

Poty, B., Leroy, J., Cathelineau, M., Cuney, M., Friedrich, M., Lespinasse, M., & Turpin, L. (1986). *Uranium deposits spatially related to granites in the French part of the Hercynian orogen*. Vienna: Vein type uranium deposits IAEA.

Rhede, D., Wendt, I., & Förster, H. J. (1996). A three-dimensional method for calculating independent chemical U/Pb- and Th/Pb-ages of accessory minerals. *Chemical Geology*, *130*, 247–253.

Rimsaite, J. (1982). Mineralogical and petrochemical properties of the heterogeneous granitoid rocks from radioactive occurrences in the Grenville Structural Province, Ontario and Quebec. In Y. T. Maurice (Ed.), *Uranium in granites* (pp. 81–23). Geological Survey of Canada: Paper.

Rinker, M. J., Nesbitt, H. W., & Pratt, A. R. (1997). Marcasite oxidation in low-temperature acidic (pH 3) solutions: Mechanism and rate laws. *American Mineralogist*, *82*, 900–912.

Robinson, S. C. (1960). Economic uranium deposits in granitic dykes, Bancroft district, Ontario. *The Canadian Mineralogist*, *6*, 513–521.

Robinson, S. C., & Sabina, A. P. (1955). Uraninite and thorianite from Ontario and Quebec. *American Mineralogist*, *40*, 624–633.

Sano, Y., Oyama, T., Terada, K., & Hidaka, H. (1999). Ion microprobe U-Pb dating of apatite. *Chemical Geology*, *153*, 249–258.

Santosh, M., Yokoyama, K., Biju-Sekhar, S., & Rogers, J. J. W. (2003). Multiple tectonothermal events in the granulite block of Southern India revealed from EPMA dating: Implications on the history of supercontinent. *Gondwana Research*, *6*, 27–61.

Simons, D. S., Chi, P. H., Kahora, P. M., Lux, G. E., Moore, J. L., Novak, S. W., Schwartz, C., Schwarz, S. A., Stevie, F. A. & Wilson, R. G. (1990). *Are relative sensitivity factors transferable among SIMS instruments?* Proceedings of the 7th International SIMS Conference, Monterey, CA, 111–114.

Sonet, J. (1967). Contribution à l'étude géochronologique du massif de Mortagne (Vendée). *Comptes Rendus de l'Académie des Sciences*, *262*, 15–17.

Song, B., Nutman, A. P., Dunyi, L., & Jiashan, W. (1996). 3800 to 2500 Ma crustal evolution in the Anshan area of Liaoning Province, northeastern China. *Precambrian Research*, *78*, 79–94.

Stern, R. A. (1998). High-resolution SIMS determination of radiogenic tracer-isotope ratios in minerals. In L. J. Cabri & D. J. Vaughan (Eds.), *Modern approaches to ore and environmental mineralogy*. *Short Course Series 27*. (pp. 421). Québec, Canada: Mineralogical Association of Canada.

Stern, R. A., & Amelin, Y. (2003). Assessment of errors in SIMS zircon U-Pb geochronology using a natural zircon standard and NIST SRM 610 glass. *Chemical Geology*, *197*, 111–142.

Stormer, J. C., Pierson, M. L., & Tacker, R. C. (1993). Variation of F and cl X-ray intensity due to anisotropic diffusion in apatite during electron microprobe analysis. *American Mineralogist*, *78*, 641–648.

Suzuki, K., & Adachi, M. (1991). Precambrian provenance and Silurian metamorphism of the Tsubonosawa paragneiss in the South Kitakami terrane, Northeast Japan, revealed by the chemical Th-U-total Pb isochron ages of monazite, zircon and xenotime. *Geochemical Journal*, *25*, 357–376.

Suzuki, K., & Adachi, M. (1994). Middle Precambrian detrital monazite and zircon from the Hida gneiss on Oki-Dogo Island, Japan: Their origin and implications for the correlation of basement gneiss of Southwest Japan and Korea. *Tectonophysics*, *235*, 277–292.

Suzuki, K., Adachi, M., & Kajizuka, I. (1994). Electron microprobe observations of Pb diffusion in metamorphosed detrital monazite. *Earth and Planetary Science Letters*, *128*, 391–405.

Suzuki, K., Adachi, M., & Tanaka, T. (1991). Middle Precambrian provenance of Jurassic sandstone in the Mino Terrane, central Japan: Th-U-total Pb evidence from an electron microprobe monazite study. *Sedimentary Geology*, *75*, 141–147.

Takahashi, Y., Yoshida, H., Sato, N., Hama, K., Yusa, Y., & Shimizu, H. (2002). W- and M-type tetrad effects in REE patterns for water-rock systems in the Tono uranium deposit, central Japan. *Chemical Geology*, *184*, 311–335.

Vidal, P. (1973). Premières données géochronologiques sur les granites hercyniens au Sud du Massif armoricain. *Bulletin de la Société Géologique de France*, *7*(15), 239–245.

Vidal, P. (1980). L'évolution polyorogénique du Massif Armoricain: apport de la géochronologie et de la géochimie isotopique du strontium. *Mémoires de la Société Géologique et Minéralogique de Bretagne*, *21*, 162.

Wiersma, C. L., & Rimstidt, J. D. (1984). Rates of reaction of pyrite and marcasite with ferric iron at pH 2. *Geochimica et Cosmochimica Acta*, *48*, 85–92.

Williams, I. S. (1998). U-Th-Pb geochronology by ion microprobe. In M. A. McKibben & W. C. Shanks (Eds.), *Applications of microanalytical techniques to understanding mineralizing processes*, *reviews in economic geology 7*. Littleton, CO: Society of Economic Geologists.

Williams, I. S., Buick, I. S., & Cartwright, I. (1996). An extended episode of early Mesoproterozoic metamorphic fluid flow in the Reynolds Range, central Australia. *Journal of Metamorphic Geology*, *14*, 29–47.

Wingate, M. T. D., Campbell, I. H., Compston, W., & Gibson, G. M. (1998). Ion microprobe U-Pb ages for Neoproterozoic basaltic magmatism in south-central Australia and implications for the breakup of Rodinia. *Precambrian Research*, *87*, 135–159.

Yershov, V. M. (1974). A method of examining the diffusion parameters of lead in uranium minerals. *Geochemistry International*, *10*, 1565–1568.

Yokoyama, K., Shigeoka, M., Otomo, Y., Tokuno, K., & Tsutsumi, Y. (2016). Uraninite and thorite ages of around 400 granitoids in the Japanese Islands. *Memoirs of the National Museum of Nature and Science*, *51*, 1–24.

SUPPORTING INFORMATION

Additional supporting information may be found online in the Supporting Information section at the end of this article.

How to cite this article: Horie K, Hidaka H. Development of U–Pb dating of uraninite using a secondary ion mass spectrometer: Selection of reference material and establishment of calibration method. *Island Arc*. 2019;e12319. https://doi.org/10.1111/iar.12319